J. Fluid Mech. (2018), *vol.* 836, R2, doi:10.1017/jfm.2017.786

JFM RAPIDS
journals.cambridge.org/rapids

How surface roughness reduces heat transport for small roughness heights in turbulent Rayleigh–Bénard convection

Yi-Zhao Zhang[1], **Chao Sun**[2], **Yun Bao**[3] **and Quan Zhou**[1,†]

[1]Shanghai Institute of Applied Mathematics and Mechanics and Shanghai Key Laboratory of Mechanics in Energy Engineering, Shanghai University, Shanghai 200072, China

[2]Center for Combustion Energy and Department of Thermal Engineering, Tsinghua University, 100084 Beijing, China

[3]Department of Mechanics, Sun Yat-Sen University, Guangzhou 510275, China

(Received 10 September 2017; revised 25 October 2017; accepted 28 October 2017; first published online 11 December 2017)

Rough surfaces have been widely used as an efficient way to enhance the heat-transfer efficiency in turbulent thermal convection. In this paper, however, we show that roughness does not always mean a heat-transfer enhancement, but in some cases it can also reduce the overall heat transport through the system. To reveal this, we carry out numerical investigations of turbulent Rayleigh–Bénard convection over rough conducting plates. Our study includes two-dimensional (2D) simulations over the Rayleigh number range $10^7 \leqslant Ra \leqslant 10^{11}$ and three-dimensional (3D) simulations at $Ra = 10^8$. The Prandtl number is fixed to $Pr = 0.7$ for both the 2D and the 3D cases. At a fixed Rayleigh number Ra, reduction of the Nusselt number Nu is observed for small roughness height h, whereas heat-transport enhancement occurs for large h. The crossover between the two regimes yields a critical roughness height h_c, which is found to decrease with increasing Ra as $h_c \sim Ra^{-0.6}$. Through dimensional analysis, we provide a physical explanation for this dependence. The physical reason for the Nu reduction is that the hot/cold fluid is trapped and accumulated inside the cavity regions between the rough elements, leading to a much thicker thermal boundary layer and thus impeding the overall heat flux through the system.

Key words: convection, turbulent convection, turbulent flows

1. Introduction

Turbulent convection over a rough surface is a common scenario that one often encounters in nature and in many industrial processes. For example, it can be found in

† Email address for correspondence: qzhou@shu.edu.cn

the urban atmospheric boundary layer (BL), where the urban surfaces are in general not smooth, and in the deep oceans, where the sea beds and the ocean floors always have rough topographies. It is of great interest and especially useful to reveal the properties of this type of flow. In the field of fundamental research, Rayleigh–Bénard (RB) convection, i.e. a working fluid layer in a closed system heated from below and cooled from above, has long been proposed as a classical and yet simple paradigm to study the convection phenomenon (Ahlers, Grossmann & Lohse 2009; Lohse & Xia 2010; Chillà & Schumacher 2012; Sun & Zhou 2014). Rayleigh–Bénard convection has also been adopted as an ideal model system to search for ways to enhance the heat transport of natural convection (Jin & Xia 2008; Zhong, Funfschilling & Ahlers 2009*a*; Zhong *et al.* 2009*b*; Biferale *et al.* 2012; Huang *et al.* 2013; Lakkaraju *et al.* 2013). Here, the convective heat transport is usually expressed in terms of the Nusselt number Nu, which is determined largely by the control parameters of the convection system, namely the Rayleigh number Ra and the Prandtl number Pr, defined as

$$Ra = \frac{\alpha g \Delta H^3}{\nu\kappa} \quad \text{and} \quad Pr = \frac{\nu}{\kappa}, \tag{1.1a,b}$$

where Δ is the temperature difference across the fluid layer of height H, g is the acceleration due to gravitation, and α, ν and κ are respectively the thermal expansion coefficient, the kinematic viscosity and the thermal diffusivity of the convecting fluid. Effective increase of convective heat transfer is of vital importance in many engineering applications, and the introduction of wall roughness has been expected to be an effective means for this. To study the fundamentals of heat transfer over rough surfaces, many experimental (Shen, Tong & Xia 1996; Du & Tong 1998; Ciliberto & Laroche 1999; Du & Tong 2000; Roche *et al.* 2001; Qiu, Xia & Tong 2005; Zhou & Xia 2010; Tisserand *et al.* 2011; Salort *et al.* 2014; Wei *et al.* 2014; Jiang *et al.* 2017; Xie & Xia 2017), numerical (Stringano, Pascazio & Verzicco 2006; Shishkina & Wagner 2011; Wagner & Shishkina 2015; Jiang *et al.* 2017; Toppaladoddi, Succi & Wettlaufer 2017; Zhu *et al.* 2017) and theoretical (Villermaux 1998; Shishkina & Wagner 2011; Goluskin & Doering 2016) studies on turbulent RB convection over rough plates have been carried out. Up to now, it has been widely accepted that the introduction of roughness on conducing plates could efficiently enhance the heat transport through the RB system. However, Shishkina & Wagner (2011) recently proposed that the heat transport can also be reduced due to the decrease of the effective Ra when the distances between the roughness elements are very small (see also figure 16 of Stringano *et al.* 2006). The reduction of the Nu in the presence of rough conducting plates is counterintuitive and yet interesting. We note that there is still a lack of systematic studies on this issue, and the objective of the present paper is to fill this gap.

The remainder of this paper is organized as follows. We first briefly describe the numerical methods adopted in § 2. Section 3 presents and analyses the results for heat transport obtained in rough cells and reveals the mechanism for the observed reduction of the Nu. Finally, the work is concluded in § 4.

2. Numerical methods

We carry out direct numerical simulations (DNS) of turbulent RB convection over triangularly rough conducting plates in a two-dimensional (2D) box of height $H = 1$ and horizontal length $L = 1$, as shown in figure 1(*a*). The triangular roughness elements have a vertex angle of 90° and their height and base width are h and $2h$

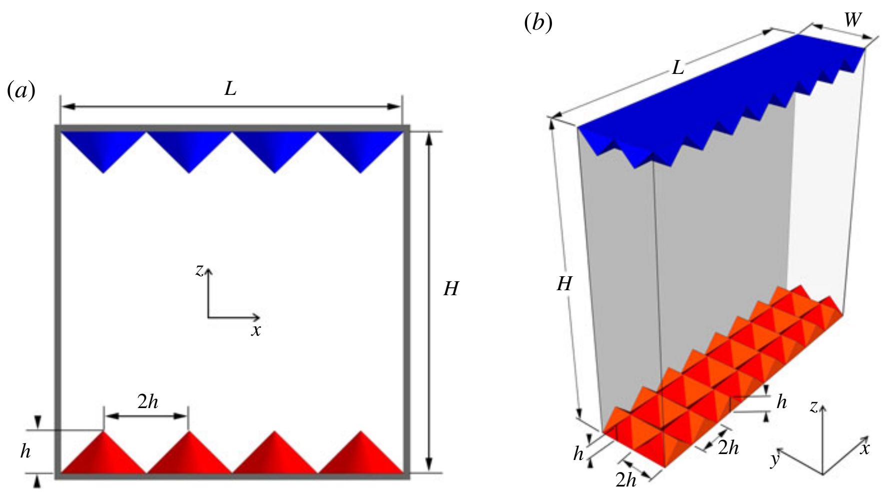

FIGURE 1. Sketches of the (*a*) 2D and (*b*) 3D convection cells with the coordinate systems. Roughness elements of height h and base width $2h$ are located on each of the plates.

respectively. In addition, three-dimensional (3D) DNS are performed in a rectangular cell of height $H = 1$, length $L = 1$ and width $W = 1/4$ (see figure 1*b*). V-shaped grooves with a vertex angle of 90° and with height h and base width $2h$ are woven on each plate, along both the L and the W directions. The influence of surface roughness on heat transport is systematically studied by varying the roughness height h. For the preset configurations, the contact area of the rough upper and lower surfaces is increased by a factor of $\sqrt{2}$. When varying h, the contact area is fixed and thus will not contribute to the variation in the Nu for both 2D and 3D situations.

The dimensionless incompressible Oberbeck–Boussinesq equations, i.e.

$$\frac{\partial \boldsymbol{u}}{\partial t} + (\boldsymbol{u} \cdot \boldsymbol{\nabla})\boldsymbol{u} = -\boldsymbol{\nabla} p + \sqrt{\frac{Pr}{Ra}}\nabla^2 \boldsymbol{u} + \theta \boldsymbol{z}, \tag{2.1}$$

$$\boldsymbol{\nabla} \cdot \boldsymbol{u} = 0, \tag{2.2}$$

$$\frac{\partial \theta}{\partial t} + (\boldsymbol{u} \cdot \boldsymbol{\nabla})\theta = \sqrt{\frac{1}{RaPr}}\nabla^2 \theta, \tag{2.3}$$

were solved using a fourth-order finite-difference scheme with staggered grids. Here, $\boldsymbol{u}$, θ and p are respectively the velocity, temperature and kinematic pressure fields and $\boldsymbol{z}$ is the unit vector along the vertical direction. Our numerical code has been extensively validated and adopted in previous studies (Bao *et al.* 2015; Chen *et al.* 2017). No-penetration and no-slip boundary conditions were applied to all solid boundaries for the velocity fields. For temperature, the vertical sidewalls were chosen to be adiabatic (no flux), while the temperature was fixed at $\theta_{cold} = -0.5$ and $\theta_{hot} = 0.5$ for the upper and lower rough plates respectively, and thus the temperature difference across the fluid layer was $\Delta = \theta_{hot} - \theta_{cold} = 1$. An immersed boundary method was applied to track the boundaries of the roughness elements (Fadlun *et al.* 2000). We simulated over the range $10^7 \leqslant Ra \leqslant 10^{11}$ for 2D cases, while Ra was fixed at 10^8 for 3D cases. In both the 2D and the 3D simulations, $Pr = 0.7$, corresponding to a working fluid of air (du Puits *et al.* 2014). Non-equidistant meshes were implemented and the

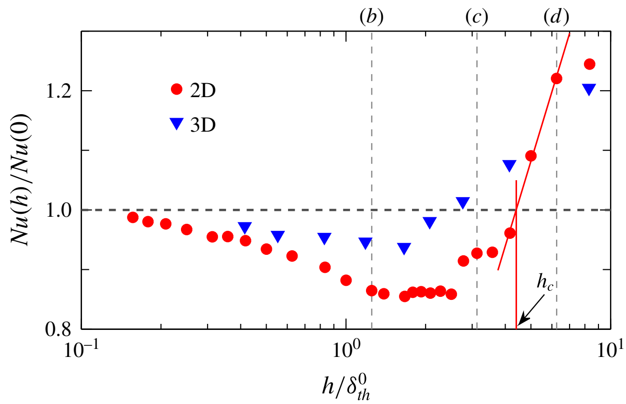

FIGURE 2. The ratio $Nu(h)/Nu(0)$ as a function of the normalized roughness height h/δ_{th}^0 obtained at $Ra = 10^8$ for 2D (triangles) and 3D (circles) simulations. Here, δ_{th}^0 is the thermal BL thickness obtained in the smooth cell using $\delta_{th}^0 = 1/[2Nu(0)]$. The red solid lines show the determination of h_c, which is the roughness height at which $Nu(h_c)/Nu(0) = 1$. The three vertical dashed lines mark the roughness heights that correspond respectively to figure 3(*b*–*d*).

computational meshes were refined close to all solid surfaces. The grid resolution was chosen to reveal all scales of turbulent convection (Shishkina *et al.* 2010) and the thermal BLs were resolved with at least 16 grid points for all runs. Specifically, 2560×3456 grid points were used for $Ra = 10^{11}$ (2D) and $512 \times 128 \times 624$ for $Ra = 10^8$ (3D).

3. Results and discussion

We first study the effects of roughness on the measured Nusselt number Nu, which is calculated as $Nu = \sqrt{RaPr}\langle w\theta\rangle - \langle \partial\theta/\partial z\rangle$, where w is the vertical component of the velocity field and $\langle\cdot\rangle$ indicates the average over time and over the mid-height horizontal plane. We checked that the variation in Nu calculated at different vertical positions in the core part of the convection cell between the roughness elements was smaller than 1 % for all of the simulations. All statistics were collected over more than 500 free-fall time units after the convective flow in the cell had been fully developed. Figure 2 shows the measured Nu as a function of the normalized roughness height h/δ_{th}^0, obtained at $Ra = 10^8$ for both the 2D and the 3D results. Here, $Nu(h)$ is normalized by $Nu(h = 0)$ of the smooth cell to show the enhancement/reduction effects, and δ_{th}^0 is the thermal BL thickness for the smooth wall case estimated from $\delta_{th}^0 = 1/[2Nu(0)]$. Despite the different magnitudes, both data sets exhibit some kind of similar trend, i.e. $Nu(h)$ first decreases at small roughness heights, reaches a minimum and then increases. Two different regimes can be identified: the Nu reduction regime where the overall heat transport is depressed and the Nu enhancement regime where an increase of heat flux is achieved. The division between the two regimes gives a critical roughness height h_c at which $Nu(h)$ crosses the value of $Nu(h = 0)$, as shown by the red solid lines in figure 2. The observed reduction in $Nu(h)$ is quite counterintuitive: now the increased contact area provided by the rough surfaces does not promote the heat flux but rather impedes it. It should be noted that Du & Tong (1998) found that the effect of rough walls on Nu is negligible if the height of the roughness elements is smaller than the thermal BL thickness for the smooth wall case.

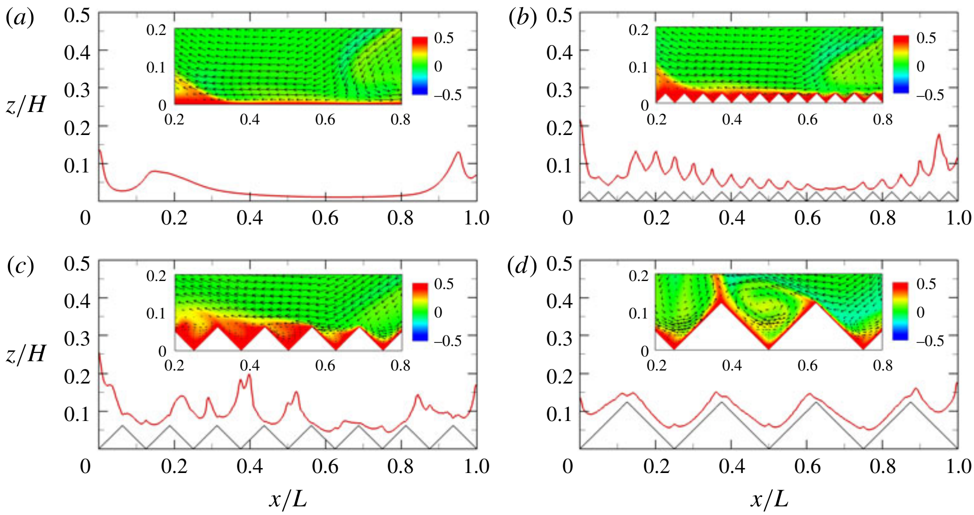

FIGURE 3. The thermal BL thicknesses, $\delta_{th}(x)$ (red curves), in the z-direction near the bottom plate as a function of the horizontal position x/L, determined from the time-averaged temperature profiles using the 'slope' method (Zhou & Xia 2013) and obtained at $Ra = 10^8$ for 2D simulations. The insets show the corresponding instantaneous snapshots of the temperature (colour) and velocity (arrows) fields near the centre of the bottom plate. The data are obtained in the smooth cell (*a*) and in the rough cells with triangular roughness elements (black lines) of height h/h_c = (*b*) 0.28, (*c*) 0.71 and (*d*) 1.42. The corresponding movie is available in the supplementary material (https://doi.org/10.1017/jfm.2017.786).

One would thus expect $Nu(h)/Nu(0) \approx 1$ for $h/\delta^0_{th} \lesssim 1$. In the present study, however, $Nu(h)/Nu(0) < 1$ is clearly observed over the range $h/\delta^0_{th} < 2.5$ ($h/\delta^0_{th} < 4.4$) with a maximal reduction of 6.3 % (15 %) for the 3D (2D) simulations (at $Ra = 10^8$; see figure 2). It is really surprising that Nu is suppressed in such a wide parameter regime.

What is the physical reason for heat-transfer reduction by roughness surfaces? We note that for the present parameter ranges the convective flow is still in the so-called 'classical' regime (Zhu *et al.* 2017) where the global convective heat transport is restricted mainly by thermal BLs (Ahlers *et al.* 2009). This prompts us to directly investigate the spatial distribution of thermal BL thicknesses, $\delta_{th}(x)$, in the cells with and without roughness. Figures 3(*a*) and 4(*a*) show, for the 2D and 3D simulations respectively, $\delta_{th}(x)$ along the bottom plate obtained at $Ra = 10^8$ in the smooth cells. Here, δ_{th} is determined using the 'slope' method (Zhou & Xia 2013), i.e. the position at which the tangent of the time-averaged temperature profile at the plate crosses the bulk temperature. Due to the rising plumes near the sidewalls and the strong shear induced by the large-scale circulation (LSC), the thermal BL is thicker at the two ends but much thinner in the central regions.

Figures 3(*b*) and 4(*b*) display the horizontal distributions of δ_{th} obtained in rough cells with $h/h_c = 0.28$ (2D) and $h/h_c = 0.34$ (3D), which are both within the Nu reduction regime. Compared with the respective smooth cases, variations with x/L of scale h are imposed on δ_{th} over the rough surfaces, i.e. δ_{th} reaches a local minimum at the tips of the roughness elements, while a local maximum of δ_{th} occurs above the valleys of the cavity regions between the adjacent rough elements. To reveal how

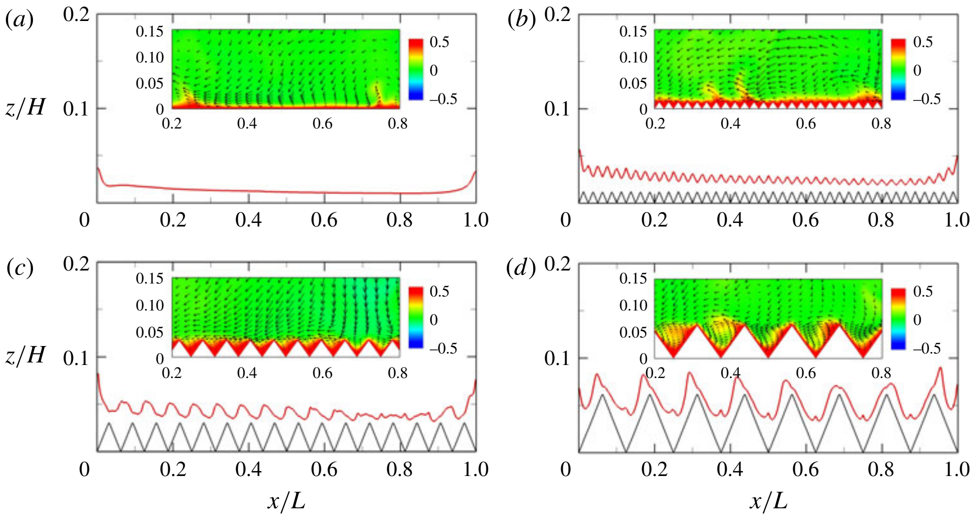

FIGURE 4. The thermal BL thicknesses, $\delta_{th}(x)$ (red curves), as a function of x/L, taken at $y=W/2$ near the bottom plate and at $Ra=10^8$ for 3D simulations. The insets show the corresponding instantaneous snapshots of the temperature (colour) and velocity (arrows) fields within the vertical plane at $y=W/2$. The data are obtained in the smooth cell (*a*) and in the rough cells with roughness heights $h/h_c=$ (*b*) 0.34, (*c*) 0.84 and (*d*) 1.68.

these patterns are developed, we look closely into the flow structures near the bottom plate, as illustrated in the insets of figures 3(*b*) and 4(*b*). It is seen that the hot fluid is trapped inside the cavity regions. Due to the relatively low Ra or small h, the flow in the cavities is dominated by the viscosity of the fluid and the trapped hot fluid cannot be well mixed, i.e. the flow in the bulk cannot penetrate into the cavities. The accumulation of the hot fluid thus thickens the thermal BLs in the cavity regions and correspondingly impedes the global heat transport through the system. The same processes can be observed for the cold fluid near the top plate. This explains why the heat transport is reduced by the roughness. It should be noted that the present mechanism of heat-flux reduction is quite similar to that of drag reduction by riblets in turbulent channel flow (Choi, Moin & Kim 1993) and in turbulent Taylor–Couette flow (Zhu *et al.* 2016). Figures 3(*c*) and 4(*c*) show the results for δ_{th} at $h/h_c=0.71$ (2D) and 0.84 (3D). As h is increased, the flow inside the cavities becomes stronger and some secondary vortices start to be generated by the LSC. However, at these values of h, the secondary vortices are too still weak to efficiently mix the fluid in all cavities and in the bulk. Therefore, the global heat transport is still less than that in the smooth wall case.

Figures 3(*d*) and 4(*d*) show δ_{th} as a function of x/L at $h/h_c=1.42$ (2D) and 1.68 (3D) respectively. Within this Nu enhancement regime, the roughness height h (and the interspace) is so large or Ra is so high that the cavities between the rough elements are accessible by the large-scale flows near the BLs. Correspondingly, the secondary vortices inside the cavities become more turbulent and thus mix the fluid vigorously. This results in a much thinner thermal BL that covers the rough surfaces uniformly, and triggers much stronger and more frequent plume emissions. Furthermore, the effective surface area is increased thanks to these roughness elements, resulting in a larger efficient heat exchange compared with that in the smooth wall case (Toppaladoddi *et al.* 2017; Zhu *et al.* 2017).

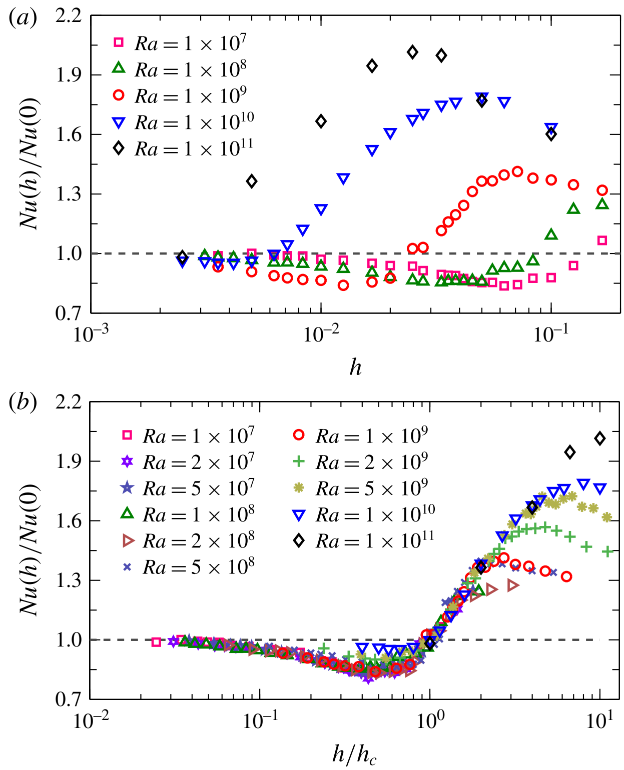

FIGURE 5. The ratio of $Nu(h)/Nu(0)$ as a function of (*a*) h and (*b*) h/h_c for Ra varying from 10^7 to 10^{11} for 2D simulations.

Figure 5(*a*) shows the ratio $Nu(h)/Nu(0)$ as a function of h for five different values of Ra. The existence of the Nu reduction regime is rather robust and it can be found for all our values of Ra studied. Nevertheless, the regime shifts towards smaller h when Ra is increased, suggesting that the reduction of Nu occurs more easily at lower Ra. Indeed, for $Ra = 10^{11}$, only a very tiny depression of Nu is measured at very small h (i.e. $Nu(h)/Nu(0) = 0.982$ at $h = 0.0025$; see the black diamonds in figure 5(*a*)). To better compare the measured $Nu(h)$ at different Ra, we adopt h_c to normalize the data, and the results are plotted in figure 5(*b*). It is seen that in the Nu reduction regime ($h/h_c \leqslant 1$), nearly all symbols can collapse on top of each other for $Ra \leqslant 10^9$, indicating that h_c is indeed a relevant typical length scale for the problem. The Nu reduction regime seems to become less pronounced with increasing Ra for $Ra > 10^9$, and may even disappear for very large Ra. In the Nu enhancement regime ($h/h_c > 1$), all $Nu(h)$ seem to grow with h in a similar trend. The maximal relative heat-transfer enhancement is larger for higher Ra, which can be explained by the fact that the roughness may trigger stronger plume emissions at higher Ra (Du & Tong 1998). At large h/h_c, one sees clearly that the value of $Nu(h)/Nu(0)$ does not increase any more. This fact of stagnation of the heat-transport enhancement may be attributed to the transition from the bulk-controlled regime to the BL-dominated regime, as proposed in the recent work of Zhu *et al.* (2017).

It is clear that the critical h_c is different for different values of Ra, i.e. h_c decreases with increasing Ra, as shown in figure 6. The question relates to which parameter in

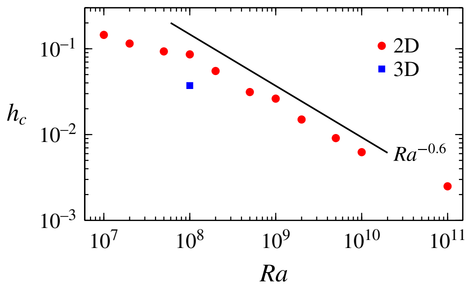

FIGURE 6. Log–log plot of h_c as a function of Ra for 2D (red circles) simulations. The solid line marks the scaling $Ra^{-0.6}$ for reference. For comparison, the value of h_c obtained at $Ra = 10^8$ in 3D cases is also plotted (blue square).

the system determines this critical roughness height h_c. To quantitatively understand this dependence, we note that the fluid inside the cavity regions is mainly subject to two forces, i.e. the viscous force, $\nu U/h_c^2$, due to the viscosity of the fluid, and the inertial force, U^2/h_c, connected to the secondary flow in the cavities, where U is the typical velocity of the LSC. When the roughness height h (and the interspace) is small (or for small Ra), the viscous force is dominant and the hot/cold fluid inside the cavity regions cannot be well mixed, thus resulting in a reduction of Nu. On the other hand, for large roughness height h (or for high Ra), the inertial force becomes strong enough to generate smaller vortices, which leads to the strong mixing in the cavity regions (see also (Zhu *et al.* 2017)) and correspondingly enhances the heat-exchange efficiency of the system. Therefore, at the critical roughness height h_c, one should expect a balance between the two forces, i.e. $\nu U/h_c^2 \sim U^2/h_c$. We hence obtain $h_c \sim \nu/U = Re^{-1}$. According to previous results of $Re \sim Ra^{0.6}$ in 2D RB flows (Sugiyama *et al.* 2009; Zhang, Zhou & Sun 2017), this yields $h_c \sim Ra^{-0.6}$, which correctly reflects the trend in figure 6, at least within the range of $10^8 \leqslant Ra \leqslant 10^{10}$.

4. Conclusion

In summary, we have demonstrated that roughness does not always cause a heat-transfer enhancement. When the roughness height h is small or Ra is low, the hot/cold fluid can be trapped inside the cavities between the rough elements, thicken the thermal BL in these regions and consequently suppress the global heat transport through the RB system. The present results suggest that special care should be taken when applying rough surfaces to enhance the convective heat transfer.

The viscous effects become more important as Pr increases or Ra decreases, which would lead to an increase of h_c. This is consistent with our dimensional arguments, i.e. $h_c \sim Re^{-1}$, as previous numerical studies have shown that Re decreases with increasing Pr or with decreasing Ra, for both 2D and 3D situations (van der Poel, Stevens & Lohse 2013). In particular, for very small Pr or for very large Ra, h_c should be too small to observe the Nu reduction. On the other hand, for large enough Pr or for small enough Ra, very large h_c is required to enhance the global heat transport. Due to the limitation of the cell height, however, heat-transport enhancement may not be achieved by surface roughness in this situation.

It should be noted that due to the lack of fluid motion in the third direction, the hot/cold fluid is more easily trapped within the cavity regions in two dimensions. This would result in a more pronounced Nu reduction and a larger h_c in the 2D simulations compared with those in the 3D simulations, as one can see in figures 2 and 6. It should also be noted that in most previous experimental studies, like that of Du & Tong (1998), no *Nu* reduction was observed in rough cells. This may be attributed to the different configurations of the rough elements. For example, Du & Tong (1998) adopted pyramids as the rough elements, which have a convex geometry that can hardly trap the hot/cold fluid, while in our present study, a concave surface was chosen as the rough configuration (see figure 1*b*). The concave rough surfaces make it possible for the hot/cold fluid to be trapped or accumulated inside the cavity regions, which should be the origination of the observed *Nu* reduction.

Acknowledgement

This work was supported by Natural Science Foundation of China under grant nos 11572185, 11672156, 11732010 and 11772362.

Supplementary movie

Supplementary movie is available at https://doi.org/10.1017/jfm.2017.786.

References

AHLERS, G., GROSSMANN, S. & LOHSE, D. 2009 Heat transfer and large scale dynamics in turbulent Rayleigh–Bénard convection. *Rev. Mod. Phys.* **81**, 503–537.

BAO, Y., CHEN, J., LIU, B.-F., SHE, Z.-S., ZHANG, J. & ZHOU, Q. 2015 Enhanced heat transport in partitioned thermal convection. *J. Fluid Mech.* **784**, R5.

BIFERALE, L., PERLEKAR, P., SBRAGAGLIA, M. & TOSCHI, F. 2012 Convection in multiphase fluid flows using lattice Boltzmann methods. *Phys. Rev. Lett.* **108**, 104502.

CHEN, J., BAO, Y., YIN, Z.-X. & SHE, Z.-S. 2017 Theoretical and numerical study of enhanced heat transfer in partitioned thermal convection. *Intl J. Heat Mass Transfer* **115**, 556–569.

CHILLÀ, F. & SCHUMACHER, J. 2012 New perspectives in turbulent Rayleigh–Bénard convection. *Eur. Phys. J.* E **35**, 58.

CHOI, H., MOIN, P. & KIM, J. 1993 Direct numerical simulation of turbulent flow over riblets. *J. Fluid Mech.* **255**, 503–539.

CILIBERTO, S. & LAROCHE, C. 1999 Random roughness of boundary increases the turbulent convection scaling exponent. *Phys. Rev. Lett.* **82**, 3998–4001.

DU, Y.-B. & TONG, P. 1998 Enhanced heat transport in turbulent convection over a rough surface. *Phys. Rev. Lett.* **81**, 987–990.

DU, Y.-B. & TONG, P. 2000 Turbulent thermal convection in a cell with ordered rough boundaries. *J. Fluid Mech.* **407**, 57–84.

FADLUN, E. A., VERZICCO, R., ORLANDI, P. & MOHD-YUSOF, J. 2000 Combined immersed-boundary/finite-difference methods for three-dimensional complex flow simulations. *J. Comput. Phys.* **161**, 35–60.

GOLUSKIN, D. & DOERING, C. R. 2016 Bounds for convection between rough boundaries. *J. Fluid Mech.* **804**, 370–376.

HUANG, S.-D., KACZOROWSKI, M., NI, R. & XIA, K.-Q. 2013 Confinement-induced heat transport enhancement in turbulent thermal convection. *Phys. Rev. Lett.* **111**, 104501.

JIANG, H.-C., ZHU, X.-J., MATHAI, V., VERZICCO, R., LOHSE, D. & SUN, C. 2017 Controlling heat transport and flow structures in thermal turbulence using ratchet surfaces. *Phys. Rev. Lett.* (submitted).

JIN, X.-L. & XIA, K.-Q. 2008 An experimental study of kicked thermal turbulence. *J. Fluid Mech.* **606**, 133–151.

LAKKARAJU, R., STEVENS, R. J. A. M., ORESTA, P., VERZICCO, R., LOHSE, D. & PROSPERETTI, A. 2013 Heat transport in bubbling turbulent Rayleigh–Bénard convection. *Proc. Natl. Acad. Sci. USA* **110**, 9237–9242.

LOHSE, D. & XIA, K.-Q. 2010 Small-scale properties of turbulent Rayleigh–Bénard convection. *Annu. Rev. Fluid Mech.* **42**, 335–364.

VAN DER POEL, E. P., STEVENS, R. J. A. M. & LOHSE, D. 2013 Comparison between two- and three-dimensional Rayleigh–Bénard convection. *J. Fluid Mech.* **736**, 177–194.

DU PUITS, R., LI, L., RESAGK, C. & THESS, A. 2014 Turbulent boundary layer in high Rayleigh number convection in air. *Phys. Rev. Lett.* **112**, 124301.

QIU, X.-L., XIA, K.-Q. & TONG, P. 2005 Experimental study of velocity boundary layer near a rough conducting surface in turbulent natural convection. *J. Turbul.* **6**, 30.

ROCHE, R.-E, CASTAING, B., CHABAUD, B. & HEBRAL, B. 2001 Observation of the 1/2 power law in Rayleigh–Bénard convection. *Phys. Rev.* E **63**, 045303(R).

SALORT, J., LIOT, O., RUSAOUEN, E., SEYCHELLES, F., TISSERAND, J.-C., CREYSSELS, M., CASTAING, B. & CHILLÀ, F. 2014 Thermal boundary layer near roughnesses in turbulent Rayleigh–Bénard convection: flow structure and multistability. *Phys. Fluids* **26**, 015112.

SHEN, Y., TONG, P. & XIA, K.-Q. 1996 Turbulent convection over rough surfaces. *Phys. Rev. Lett.* **76**, 908–911.

SHISHKINA, O., STEVENS, R. J. A. M., GROSSMANN, S. & LOHSE, D. 2010 Boundary layer structure in turbulent thermal convection and its consequences for the required numerical resolution. *New J. Phys.* **12**, 075022.

SHISHKINA, O. & WAGNER, C. 2011 Modelling the influence of wall roughness on heat transfer in thermal convection. *J. Fluid Mech.* **686**, 568–582.

STRINGANO, G., PASCAZIO, G. & VERZICCO, R. 2006 Turbulent thermal convection over grooved plates. *J. Fluid Mech.* **557**, 307–336.

SUGIYAMA, K., CALZAVARINI, E., GROSSMANN, S. & LOHSE, D. 2009 Flow organization in two-dimensional non-Oberbeck–Boussinesq Rayleigh–Bénard convection in water. *J. Fluid Mech.* **637**, 105–135.

SUN, C. & ZHOU, Q. 2014 Experimental techniques for turbulent Taylor–Couette flow and Rayleigh–Bénard convection. *Nonlinearity* **27**, R89–R121.

TISSERAND, J.-C., CREYSSELS, M., GASTEUIL, Y., PABIOU, H., GIBERT, M., CASTAING, B. & CHILLÀ, F. 2011 Comparison between rough and smooth plates within the same Rayleigh–Bénard cell. *Phys. Fluids* **23**, 015105.

TOPPALADODDI, S., SUCCI, S. & WETTLAUFER, J. S. 2017 Roughness as a route to the ultimate regime of thermal convection. *Phys. Rev. Lett.* **118**, 074503.

VILLERMAUX, E. 1998 Transfer at rough sheared interfaces. *Phys. Rev. Lett.* **81**, 4859–4862.

WAGNER, S. & SHISHKINA, O. 2015 Heat flux enhancement by regular surface roughness in turbulent thermal convection. *J. Fluid Mech.* **763**, 109–135.

WEI, P., CHAN, T.-S., NI, R., ZHAO, X.-Z. & XIA, K.-Q. 2014 Heat transport properties of plates with smooth and rough surfaces in turbulent thermal convection. *J. Fluid Mech.* **740**, 28–46.

XIE, Y.-C & XIA, K.-Q. 2017 Turbulent thermal convection over rough plates with varying roughness geometries. *J. Fluid Mech.* **825**, 573–599.

ZHANG, Y., ZHOU, Q. & SUN, C. 2017 Statistics of kinetic and thermal energy dissipation rates in two-dimensional turbulent Rayleigh–Bénard convection. *J. Fluid Mech.* **814**, 165–184.

ZHONG, J.-Q., FUNFSCHILLING, D. & AHLERS, G. 2009*a* Enhanced heat transport by turbulent two-phase Rayleigh–Bénard convection. *Phys. Rev. Lett.* **102**, 124501.

ZHONG, J.-Q., STEVENS, R. J. A. M., CLERCX, H. J. H., VERZICCO, R., LOHSE, D. & AHLERS, G. 2009*b* Prandtl-, Rayleigh-, and Rossby-number dependence of heat transport in turbulent rotating Rayleigh–Bénard convection. *Phys. Rev. Lett.* **102**, 044502.

ZHOU, Q. & XIA, K.-Q. 2010 Universality of local dissipation scales in buoyancy-driven turbulence. *Phys. Rev. Lett.* **104**, 124301.

ZHOU, Q. & XIA, K.-Q. 2013 Thermal boundary layer structure in turbulent Rayleigh–Bénard convection in a rectangular cell. *J. Fluid Mech.* **721**, 199–224.

ZHU, X., OSTILLA-MÓNICO, R., VERZICCO, R. & LOHSE, D. 2016 Direct numerical simulation of Taylor–Couette flow with grooved walls: torque scaling and flow structure. *J. Fluid Mech.* **794**, 746–774.

ZHU, X., STEVENS, R. J. A. M., VERZICCO, R. & LOHSE, D. 2017 Roughness-facilitated local 1/2 scaling does not imply the onset of the ultimate regime of thermal convection. *Phys. Rev. Lett.* **119**, 154501.